

A Closed-Form Surrogate for the Equivalent Diameter of the Kerr Shadow

Arseny Pantsialei*

Institute of Physics, Maria Curie-Skłodowska University, 20-031 Lublin, Poland

Abstract

We present a closed-form surrogate for the equivalent diameter of the Kerr black-hole shadow, defined as the diameter of the circle with the same area as the shadow's critical curve. The construction enforces the exact face-on (polar) limit by explicitly separating an analytically computed polar contribution based on the spherical photon-orbit branch where the horizontal impact parameter vanishes. The remaining inclination dependence is captured by a compact 15-parameter polynomial placed inside an exponential correction. The coefficients are determined by ordinary least squares on a deterministic reference grid generated from the Kerr critical-curve area. Over the practical domain of dimensionless spin from 0 to 0.998 and inclination from just above 0 degrees up to 90 degrees (with the exactly polar point treated analytically), the surrogate achieves sub-percent accuracy. On the training grid the median absolute percent error is 0.0105 percent with a worst case of 0.782 percent, and on a denser out-of-sample validation set (including inclinations down to 0.5 degrees) the median, 95th-percentile, and worst-case errors are 0.023 percent, 0.471 percent, and 1.64 percent, respectively. The resulting expression provides fast evaluations of the shadow size without numerical ray tracing, making it convenient for repeated calls in parameter inference and rapid model comparisons.

1 Introduction

A black-hole shadow is, at heart, a piece of geometry: it is the projection on the observer screen of the set of photon trajectories that asymptotically hover on unstable spherical orbits before escaping. Once this critical curve is known, one can extract compact, mass-independent descriptors of its size and use them as strong-field probes. For the Kerr family the curve is close to circular for a wide range of parameters,

and its overall scale is controlled mainly by the dimensionless spin a_* and the viewing inclination i .

The motivation for having such descriptors in a form that is both fast and robust is no longer academic. Horizon-scale imaging has pushed inference pipelines into regimes where the same forward model must be evaluated many times, and it is often wasteful to ray-trace an entire image when only a single scalar summary of the shadow size is needed. The Event Horizon Telescope (EHT) analyses, including polarization constraints for Sgr A* [1] and multi-epoch evidence for a persistent shadow of M87* [2, 3], make this point particularly concrete. Looking ahead, next-generation arrays are expected to access photon-ring structure more directly [4, 5], while propagation effects such as internal Faraday rotation are being bounded for Sgr A* [6]. Throughout, we stress a simple separation of roles: the surrogate developed here concerns only the geometry of the Kerr critical curve. Connecting it to specific image-domain observables inevitably requires additional astrophysical modeling.

It is also worth recalling that Kerr is not the end of the story. A large literature explores how shadow size and asymmetry respond when one departs from Kerr by adding extra charges, acceleration, or effective corrections, or by considering compact alternatives [7–14]. In such settings, explicit parametrizations of the critical curve or full ray tracing are often unavoidable. Yet even in the Kerr case, many practical inference tasks reduce to repeatedly evaluating a single size summary across a dense (a_*, i) grid, and it is precisely this repeated-evaluation bottleneck that we target.

We focus on a standard size observable. The *equivalent diameter* D_{eq} , defined as the diameter of a circle with the same area as the shadow. It is convenient to normalize out the trivial mass scaling by introducing

$$y(a_*, i) \equiv \frac{D_{\text{eq}}}{6\sqrt{3}M}, \quad (1)$$

so that lengths are measured in units of M and $y \rightarrow 1$ in the Schwarzschild limit $a_* \rightarrow 0$. The task is then

*e-mail: wselend@gmail.com

to provide an accurate closed-form approximation for $y(a_*, i)$ on the physically relevant domain.

The Kerr shadow has one feature that is too valuable to approximate numerically: the exactly polar (face-on) limit. When $i \rightarrow 0$ the critical curve becomes a circle, but its radius remains a nontrivial function of spin. We therefore factor out the polar curve $y_{\text{pole}}(a_*) \equiv y(a_*, i \rightarrow 0)$ and model only the remaining inclination dependence. Concretely, we write

$$y_{\text{fit}}(a_*, i) = y_{\text{pole}}(a_*) \exp[-x z F(x, z)], \quad x = (a_*)^2, \quad (2)$$

where $F(x, z)$ is taken to be a low-order polynomial and its coefficients are obtained by linear regression on a deterministic Kerr reference grid. This representation is convenient for two reasons. First, it preserves positivity by construction. Second, it makes the limiting structure transparent. As $z \rightarrow 0$ one has $x z F \rightarrow 0$ and hence

$$y(a_*, i \rightarrow 0) \rightarrow y_{\text{pole}}(a_*), \quad (3)$$

while as $x \rightarrow 0$ both $y_{\text{pole}} \rightarrow 1$ and $x z F \rightarrow 0$, so the Schwarzschild limit $y \rightarrow 1$ is enforced automatically. The polar curve itself is not fitted. It is evaluated *exactly* from the axial critical curve by solving a cubic equation for the relevant spherical photon orbit, so the spin-dependent face-on size is imposed analytically rather than learned from data.

Our intended application domain is the practically relevant range $a_* \in [0, 0.998]$ and $i \in [0^\circ, 90^\circ]$, with explicit validation extending down to small but nonzero inclinations. Reference values of D_{eq} are generated by a purely geometric pipeline: we compute the Kerr critical curve traced by spherical photon orbits, map it to the observer screen coordinates (α, β) , evaluate the enclosed area A , and set $D_{\text{eq}} = 2\sqrt{A/\pi}$. The surrogate is benchmarked against this grid and then tested out of sample on a denser validation set. As one might anticipate, the largest relative errors occur at very small inclinations, where the dependence on i becomes intrinsically weak and percent-level measures can over-emphasize tiny absolute deviations.

We proceed by first deriving the closed form of $y_{\text{pole}}(a_*)$ and presenting the fitted coefficients for $F(x, z)$ together with a compact accuracy summary over the full domain. A minimal external consistency check against published Kerr shadow areas is included to anchor the reference values. The computational details of the deterministic reference pipeline used to build the grid are recorded in Appendix A. Together with the explicit closed-form expression and the coefficient table, this information is sufficient to reproduce the fit and all reported accuracy statistics with an independent implementation.

2 Closed-form surrogate construction

Our goal is to approximate the normalized equivalent diameter,

$$y(a_*, i) \equiv \frac{D_{\text{eq}}}{6\sqrt{3}M}, \quad x \equiv a_*^2, \quad z \equiv \sin^2 i, \quad (4)$$

by a closed expression that respects the two physically distinguished limits: the Schwarzschild point $z = \sin^2 i$ and the polar view $i \rightarrow 0$. The simplest way to build these constraints in from the start is to separate the exactly known spin dependence in the face-on geometry from the remaining inclination dependence, and to model the latter in an exponential form. We therefore write

$$y_{\text{fit}}(x, z) = y_{\text{pole}}(a_*) \exp[-x z F(x, z)], \quad (5)$$

where $y_{\text{pole}}(a_*) \equiv y(a_*, i \rightarrow 0)$ is evaluated analytically (Sec. 2.1), and $F(x, z)$ is a low-order polynomial determined from a Kerr reference grid.

The limiting behavior is then immediate. In the polar limit $z \rightarrow 0$ the exponent vanishes, so the surrogate collapses to the exact polar curve, $y_{\text{fit}} \rightarrow y_{\text{pole}}(a_*)$. In the Schwarzschild limit $x \rightarrow 0$ we have $y_{\text{pole}} \rightarrow 1$ while the product $x z F$ again forces the exponent to zero, hence $y_{\text{fit}} \rightarrow 1$. In this sense the structure of (5) eliminates the need for any ad hoc regularization in the inclination variable. The potentially delicate regime $i \approx 0$ is handled analytically by construction, and only the genuinely two-parameter deviation away from the polar curve is fitted.

2.1 Polar limit in closed form

In the exactly axial configuration $i = 0$ the Kerr critical curve becomes a circle on the observer screen, so the shadow area is fixed once its radius is known. To determine this radius it is convenient to start from the standard screen coordinates (α, β) expressed in terms of the conserved impact parameters of spherical photon orbits, $\xi(r)$ and $\eta(r)$. The polar limit is subtle only in appearance: as $i \rightarrow 0$ the horizontal coordinate behaves as $\alpha \propto \xi / \sin i$, so a finite axial image requires $\xi = 0$. Thus the face-on shadow is controlled by the unique spherical photon orbit on the $\xi = 0$ branch, at some Boyer-Lindquist radius r_0 , and its screen radius can be written as

$$\rho_{\text{pole}}(a_*) = \sqrt{\eta(r_0) + a_*^2}, \quad \xi(r_0) = 0, \quad (6)$$

with r_0 determined implicitly by the condition $\xi(r_0) = 0$.

Imposing $\xi(r_0) = 0$ reduces the problem to a single cubic equation for r_0 ,

$$r_0^3 - 3r_0^2 + xr_0 + x = 0, \quad x \equiv a_*^2, \quad (7)$$

and physics selects the root that connects continuously to the Schwarzschild photon sphere, $r_0(0) = 3$, and remains on the admissible spherical-orbit branch throughout the practical spin range $x \in [0, 0.998^2]$. Writing the cubic in depressed form, this distinguished root admits the closed expression

$$r_0(x) = 1 + 2\sqrt{1 - \frac{x}{3}} \cos \left[\frac{1}{3} \arccos \left(\frac{3\sqrt{3}(1-x)}{(3-x)^{3/2}} \right) \right]. \quad (8)$$

Once ρ_{pole} is known, the polar shadow is simply a circle of diameter $D_{\text{eq}} = 2\rho_{\text{pole}}$, and therefore the normalized equivalent diameter in the face-on limit becomes

$$y_{\text{pole}}(a_*) = \frac{\rho_{\text{pole}}(a_*)}{3\sqrt{3}M}. \quad (9)$$

2.2 Inclination-dependent correction

Once the exact polar curve $y_{\text{pole}}(a_*)$ has been factored out, the remaining dependence on inclination is a smooth correction in the variable $z = \sin^2 i$. It is therefore natural to represent the function $F(x,z)$ by a low-order polynomial that is linear in its coefficients, so that the fit reduces to a transparent linear regression problem. In the surrogate model we use a compact 15-parameter basis, deliberately avoiding logarithms or other non-analytic structure in z :

$$F(x,z) = \sum_{m=0}^3 a_m x^m + \left(\sum_{m=0}^3 b_m x^m \right) z \quad (10)$$

$$+ \left(\sum_{m=0}^3 c_m x^m \right) z^2 + \left(\sum_{m=0}^2 d_m x^m \right) z^3. \quad (11)$$

The truncation at z^3 captures the observed smooth inclination dependence across the practical domain while keeping the surrogate genuinely lightweight: evaluating $F(x,z)$ and hence y_{fit} requires only a handful of multiplications and additions.

2.3 Reference accuracy and convergence

Before trusting any surrogate, one must first be sure that the reference values it is trained on are themselves numerically stable. We therefore performed an

explicit refinement study of the geometric reference computation. For each tested parameter pair (a_*, i) we sampled the critical curve with three resolutions $N, 2N, 4N$ and monitored the relative stabilization

$$\delta_{24} := \frac{|y_{4N} - y_{2N}|}{|y_{4N}|}, \quad (12)$$

where y is extracted from the contour area via the equivalent diameter (cf. Eq. (15)). In other words, δ_{24} measures how much the normalized size changes when the sampling density along the curve is doubled from $2N$ to $4N$.

Over the tested set spanning the full (a_*, i) domain, we find

$$\max \delta_{24} = 7.1 \times 10^{-10}, \quad N_{\text{max}} = 1.6 \times 10^4. \quad (13)$$

Accordingly, we fix the reference resolution to $N_{\text{ref}} = 1.6 \times 10^4$ for all subsequent reference evaluations. With this choice the residual numerical uncertainty of the reference grid is far below the surrogate approximation error reported in the main text and can be neglected at the level of accuracy of interest.

2.4 Fitting procedure

Let $y_{\text{ref}}(a_*, i)$ denote the reference values produced by the geometric pipeline described in Appendix A, and let $y_{\text{pole}}(a_*)$ be evaluated exactly via Eqs. (7)-(9). Since the surrogate (5) is written as an exponential correction to the polar curve, the most stable quantity to fit is the logarithmic deviation from the polar limit. For all grid points with $x > 0$ and $z > 0$ we therefore define

$$\Delta_{\text{ref}}(x, z) \equiv -\ln \left(\frac{y_{\text{ref}}(x, z)}{y_{\text{pole}}(a_*)} \right). \quad (14)$$

By construction (5) implies $\Delta_{\text{ref}}(x, z) = xzF(x, z)$. Substituting the polynomial ansatz (11) then turns the problem into a linear regression for the coefficient set $\{a_m, b_m, c_m, d_m\}$, with basis functions $\{x^m\}$, $\{x^m z\}$, $\{x^m z^2\}$, and $\{x^m z^3\}$ truncated exactly as in (11). Points with $x = 0$ or $z = 0$ are excluded only because Δ_{ref} is undefined there; the corresponding limits are not learned from data but enforced analytically by the structure of (5).

In practice we solve the resulting linear least-squares problem using a numerically stable routine (QR or SVD), rather than relying on raw normal equations. This avoids spurious coefficient growth without introducing any ad hoc inclination regularization, and it leaves the fitted accuracy across the grid unchanged at the level reported below.

3 Validation and reproducibility

To judge a surrogate fairly, one must separate two questions that are often conflated: whether the *fit* is accurate, and whether the *reference values* against which it is judged are trustworthy. We therefore describe the geometric reference computation in a way that fixes the ordering of the critical curve unambiguously, and we summarize the resulting accuracy both on the training grid and on an out-of-sample validation set. All ingredients are either analytic or generated deterministically from analytic Kerr geodesics, and the reference pipeline is specified in Appendix A.

For each parameter pair (a_*, i) with $i > 0$ we generate a reference value $y_{\text{ref}}(a_*, i)$ directly from the Kerr critical curve (Appendix A). We sample the spherical-orbit radius $r \in [r_-, r_+]$, compute the corresponding impact parameters $(\xi(r), \eta(r))$, and map them to the observer screen using the standard Kerr relations to obtain the two branches $(\alpha(r), \beta_{\pm}(r))$. The key practical point is that the critical curve is then turned into a closed polygon without any angle-sorting heuristics. We traverse the upper branch $\beta_+(r)$ from r_- to r_+ , return along the lower branch $\beta_-(r)$ from r_+ back to r_- , and concatenate these point lists. This procedure fixes the vertex ordering once and for all, so the enclosed area can be computed robustly by the shoelace formula. With the area A in hand we define

$$D_{\text{eq}} = 2\sqrt{A/\pi}, \quad y_{\text{ref}} = \frac{D_{\text{eq}}}{6\sqrt{3}M}. \quad (15)$$

The exactly polar case $i = 0^\circ$ is treated analytically through the closed-form polar curve $y_{\text{pole}}(a_*)$ (Sec. 2.1). Since our fitting target involves a logarithmic ratio to y_{pole} , the point $i = 0^\circ$ is excluded from the regression and from the error statistics below. The polar limit is enforced by construction of the surrogate.

3.1 External consistency check

Although the reference grid is generated internally, it is reassuring to anchor it against an independent tabulation. As a minimal cross-check we consider the equatorial observer, $i = 90^\circ$, and compare the shadow areas to those reported by Kumar & Ghosh [15] (their Table 1). In this case it is convenient to express the normalized equivalent diameter in terms of the area ratio to the Schwarzschild value. Since for $a_* = 0$ the shadow is a circle of radius $3\sqrt{3}M$, its area is $A_0 = 27\pi M^2$, and therefore

$$y_{\text{ref}}(a_*) \equiv \frac{D_{\text{eq}}}{6\sqrt{3}M} = \sqrt{\frac{A(a_*)}{A_0}}, \quad (16)$$

which is manifestly independent of the black-hole mass and distance. We find agreement at the $\lesssim 10^{-4}$ level for the tabulated spins, with the residual consistent with rounding in the published area values.

3.2 Accuracy on training and validation sets

We quantify the surrogate error by the relative percent deviation

$$\varepsilon(\%) \equiv 100 \frac{y_{\text{fit}} - y_{\text{ref}}}{y_{\text{ref}}}, \quad (17)$$

and report absolute errors $|\varepsilon|$. The surrogate value y_{fit} is computed from (5), with $F(x, z)$ given by (11) and coefficients listed in Table 1. The polar curve $y_{\text{pole}}(a_*)$ is evaluated exactly via Eqs. (7)-(9). All error statistics and maps refer to the domain $i > 0$, since the point $i = 0^\circ$ is handled analytically.

On the uniform training grid $a_* \in [0, 0.998]$ (26 values) and $i \in (0^\circ, 90^\circ]$ (30 values), for a total of 780 points, the absolute percent error has median 0.0105% and worst case 0.782%. On a denser out-of-sample grid (2204 points, including inclinations down to 0.5°), the median, 95th-percentile, and worst-case absolute percent errors are 0.023%, 0.471%, and 1.64%, respectively. The worst deviations occur at very small inclinations, where the shadow becomes almost circular and the dependence on i is intrinsically weak. In that regime a tiny absolute mismatch can look disproportionately large when expressed as a percentage.

Figure 1 summarizes the two complementary pieces of information one typically wants in practice: panel (a) shows the physical deviation $100(y_{\text{ref}} - 1)$ across the domain, while panel (b) shows the surrogate error $\varepsilon(\%)$ evaluated on the discrete training grid (no interpolation), excluding the analytic point $i = 0^\circ$.

3.3 Reproducibility

A surrogate is only as useful as it is reproducible. Here reproducibility is straightforward because every ingredient is either analytic or generated deterministically from analytic Kerr geodesics. The reference grids $y_{\text{ref}}(a_*, i)$ are constructed from the Kerr critical curve as described in Appendix A, with the equivalent diameter defined by the area prescription (15). The fitted coefficients are obtained by a linear regression in a numerically stable variable. For all grid points

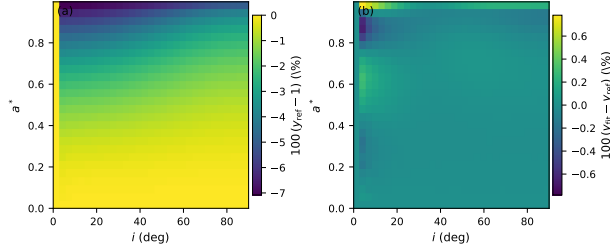


Figure 1: (a) Relative deviation $100(y_{\text{ref}} - 1)$ (%) of the Kerr shadow equivalent diameter from the Schwarzschild value $6\sqrt{3}M$. (b) Surrogate error $100(y_{\text{fit}} - y_{\text{ref}})/y_{\text{ref}}$ (%) evaluated on the discrete training grid (no interpolation), excluding the exactly polar case $i = 0^\circ$ treated analytically.

with $x > 0$ and $z > 0$ we fit the logarithmic deviation from the polar curve,

$$\Delta = -\ln\left(\frac{y_{\text{ref}}}{y_{\text{pole}}}\right) = xzF(x,z), \quad (18)$$

as discussed in Sec. 2.4. Because the construction is deterministic and the surrogate is fully specified by Eqs. (5)-(11) together with Table 1, all results reported here can be reproduced with an independent implementation. In particular, the reference grids $y_{\text{ref}}(a_*, i)$ are generated from the Kerr critical curve as described in Appendix A, and the fit is obtained by linear least squares in the stable variable $\Delta = -\ln(y_{\text{ref}}/y_{\text{pole}})$ (Sec. 2.4).

It is useful to keep in mind what this closed form does and what it does not do. The object we approximate is a single geometric descriptor, the equivalent diameter D_{eq} of the Kerr *critical curve*. We do not attempt to encode higher-order shape moments, nor do we model propagation, scattering, instrumental response, or radiative transfer. Accordingly, the surrogate is not a replacement for full imaging or ray-tracing pipelines when detailed morphology, polarization, or visibility-domain structure is required. Its role is more modest and more practical: within the stated (a_*, i) range it provides a fast analytic subroutine that can be evaluated repeatedly inside broader inference or forward-model pipelines.

This distinction matters when one connects geometry to data. In horizon-scale radio images, commonly quoted size estimators for instance, the diameter of a bright emission ring inferred from visibilities need not coincide with the geometric shadow diameter, and can depend on the emission model, optical depth, scattering, and instrumental effects. The present formula should therefore be viewed as a geometric component that can be coupled to such models, rather than as a direct observable by itself. Using D_{eq} as

a proxy for an observed ring diameter must be justified within a specified radiative-transfer and scattering framework.

A further limitation is intrinsic and cannot be removed without additional information. D_{eq} is a single scalar, so it cannot in general disentangle the two parameters (a_*, i) . Distinct pairs (a_*, i) may yield the same equivalent diameter, and breaking this degeneracy requires supplementary observables beyond the shadow area.

Finally, the regime of very small inclinations deserves a specific comment. As $i \rightarrow 0$ the shadow becomes nearly circular, so the dependence on i weakens and the size is dominated by the spin-dependent polar curve $y_{\text{pole}}(a_*)$. In that limit even tiny absolute mismatches in the inclination-dependent correction can translate into noticeable percent-level deviations. For this reason we validate explicitly on a dense grid down to $i = 0.5^\circ$ and recommend using the out-of-sample statistics as the relevant performance indicator whenever near-face-on configurations are of interest. The exactly polar point $i = 0^\circ$ itself is handled analytically through $y_{\text{pole}}(a_*)$ and is excluded from the regression fit and from the error maps.

Because the surrogate is fully specified by Eqs. (5)-(11) together with the coefficient table (Table 1), every number reported in this section can in principle be reproduced with an independent implementation, without access to our original code.

Table 1: Coefficients of the 15-parameter surrogate model defined in Eq. (11).

Coefficient	Value	Coefficient	Value
a_0	-2.9132×10^{-2}	b_0	-1.7742×10^{-2}
a_1	3.0192×10^{-2}	b_1	6.5971×10^{-2}
a_2	-7.9740×10^{-2}	b_2	-1.6888×10^{-1}
a_3	6.2570×10^{-2}	b_3	1.2776×10^{-1}
c_0	1.5303×10^{-2}	d_0	-2.0970×10^{-3}
c_1	-2.3543×10^{-2}	d_1	-2.7667×10^{-2}
c_2	1.0079×10^{-1}	d_2	3.6628×10^{-2}
c_3	-1.1297×10^{-1}		

4 Conclusion

The Kerr shadow is a piece of geometry that one often needs to evaluate many times. In this work we have distilled one widely used size descriptor—the equivalent diameter—into a compact closed form that is both numerically stable and faithful to the relevant analytic limits. Writing

$$y(a_*, i) = \frac{D_{\text{eq}}}{6\sqrt{3}M}, \quad (19)$$

we have constructed a surrogate of the form

$$y_{\text{fit}}(a_*, i) = y_{\text{pole}}(a_*) \exp[-xzF(x, z)], \quad x = a_*^2, \quad z = \frac{\sin^2 i}{\sin^2 a_*}, \quad (20)$$

so that all inclination dependence enters through a smooth polynomial $F(x, z)$, while the exactly polar contribution is factored out explicitly.

The decisive step is to treat the face-on limit analytically rather than numerically. For $i = 0$ the critical curve is a circle, but its radius remains spin dependent. This dependence is fixed by the unique spherical photon orbit on the $\xi = 0$ branch and is obtained by solving a single cubic equation. As a result, the polar curve $y_{\text{pole}}(a_*)$ is known in closed form and the correct behavior as $i \rightarrow 0$ is enforced by construction. Without any empirical fitting in a regime where percent-level errors can be misleading.

With the polar curve removed, the remaining task reduces to a transparent linear regression. We fit the coefficients of $F(x, z)$ using the logarithmic deviation

$$\Delta = -\ln\left(\frac{y_{\text{ref}}}{y_{\text{pole}}}\right) = xzF(x, z), \quad (21)$$

which is numerically stable and avoids divisions by small parameters. In particular, no logarithmic or ad hoc regularization in the inclination variable is needed. The potentially delicate small- i structure is already handled analytically by the form of the surrogate itself.

Across the fitted domain with $i > 0$, the surrogate attains sub-percent accuracy. On the training grid the absolute percent error has median 0.0105% and worst case 0.782%, while on the denser out-of-sample validation set the median, 95th-percentile, and worst-case absolute percent errors are 0.023%, 0.471%, and 1.64%, respectively. The exactly polar point $i = 0^\circ$ is excluded from the regression fit because it is treated analytically through $y_{\text{pole}}(a_*)$.

Because the final expression is closed, smooth, and inexpensive to evaluate, it is well suited for applications in which the shadow size must be computed repeatedly—for instance in parameter inference, rapid model comparison, or as a geometric module embedded within more complete forward models.

References

- [1] Event Horizon Telescope Collaboration, The Astrophysical Journal Letters **964**, L26 (2024).
- [2] Event Horizon Telescope Collaboration, Astronomy & Astrophysics **681**, A79 (2024).
- [3] Event Horizon Telescope Collaboration, Astronomy & Astrophysics **693**, A265 (2025).
- [4] P. Tiede, M. D. Johnson, D. W. Pesce, D. C. M. Palumbo, D. O. Chang, and P. Galison, Galaxies **10**, Context for future subring measurements, 111 (2022).
- [5] A. Goyal, F. Tamburini, et al., *Space-time measurements with the photon ring*, arXiv:2411.15119, 2024.
- [6] M. Wielgus, S. Issaoun, I. Martí-Vidal, et al., Astronomy & Astrophysics **682**, A97 (2024).
- [7] T.-T. Sui, Q.-M. Fu, and W.-D. Guo, Physics Letters B **845**, 138135 (2023).
- [8] F. Agurto-Sepúlveda et al., Physical Review D **110**, 024078 (2024).

- [9] X.-M. Kuang, Y. Meng, E. Papantonopoulos, and X.-J. Wang, Phys. Rev. D **110**, L061503 (2024), arXiv:2406.11932 [gr-qc].
- [10] Z. Ban, J. Chen, and J. Yang, The European Physical Journal C **85**, 10.1140/epjc/s10052-025-14614-y (2025).
- [11] S. Jana, T. Saha, and S. Chakrabarti, Physical Review D **108**, 044008 (2023).
- [12] C. Bambi, K. Freese, S. Vagnozzi, and L. Visinelli, Phys. Rev. D **100**, 044057 (2019).
- [13] S. Vagnozzi et al., Classical and Quantum Gravity **40**, 165007 (2023).
- [14] M. Khodadi, S. Vagnozzi, and J. Taghizadeh Firouzjaee, Scientific Reports **14**, 26932 (2024).
- [15] R. Kumar and S. G. Ghosh, The Astrophysical Journal **892**, 78 (2020).
- [16] L. D. Landau and E. M. Lifshitz, *The classical theory of fields*, 4th ed., Vol. 2, Course of Theoretical Physics (1975).
- [17] K. Hioki and K.-i. Maeda, Phys. Rev. D **80**, 024042 (2009).

A Deterministic reference computation

We now describe the deterministic construction of the reference equivalent diameter D_{eq} for a Kerr black hole with dimensionless spin $a_* \in [0,1]$ observed at inclination i . Since the shadow is a purely geometric object, it is convenient to work in geometric units with $G = c = 1$ and to set $M = 1$ throughout this appendix. Physical units are restored at the end by the overall scaling $(\alpha, \beta) \mapsto M(\alpha, \beta)$, which implies $A \mapsto M^2 A$ for the enclosed area and hence $D_{\text{eq}} \mapsto M D_{\text{eq}}$ for the equivalent diameter.

The starting point is the Kerr critical curve traced by spherical photon orbits. Photon trajectories are null geodesics ($ds = 0$), so their motion follows from the standard geodesic/Hamilton–Jacobi framework [16]. Null geodesics admit the conserved impact parameters

$$\xi \equiv \frac{L_z}{E}, \quad \eta \equiv \frac{\mathcal{Q}}{E^2},$$

where E is the conserved energy, L_z is the axial component of angular momentum, and \mathcal{Q} is the Carter constant. Introducing $\Delta(r) = r^2 - 2r + a_*^2$, the spherical photon orbits at Boyer-Lindquist radius r are characterized by the standard conditions $R(r) = 0$ and $R'(r) = 0$ for the radial potential. These yield

the familiar expressions

$$\xi(r) = \frac{r^2(3-r) - a_*^2(r+1)}{a_*(r-1)}, \quad (22)$$

$$\eta(r) = \frac{r^3(4a_*^2 - r^3 + 6r^2 - 9r)}{a_*^2(r-1)^2}. \quad (23)$$

Given $(\xi(r), \eta(r))$, the corresponding point on the observer screen at infinity is obtained by the standard Kerr screen map. In celestial coordinates (α, β) one has

$$\alpha(r) = -\frac{\xi(r)}{\sin i}, \quad (24)$$

$$\beta_{\pm}(r) = \pm \sqrt{\eta(r) + a_*^2 \cos^2 i - \xi(r)^2 \cot^2 i}. \quad (25)$$

Varying r along the allowed spherical-orbit interval then traces the upper and lower branches of the critical curve, $\beta_+(r)$ and $\beta_-(r)$, at fixed (a_*, i) .

The axial configuration $i \rightarrow 0$ requires a brief separate remark. The formulas (24)–(25) are written for generic inclinations and become formally singular as $\sin i \rightarrow 0$ and $\cot i \rightarrow \infty$. Physically this is not a pathology of the shadow but a reminder that axisymmetry reduces the geometry in the polar view: the critical curve becomes a circle, and only those spherical photon orbits that remain compatible with an axial line of sight contribute to it.

A convenient way to take the polar limit is to consider the sky-plane radius

$$\rho^2 \equiv \alpha^2 + \beta^2 = \eta + \xi^2 + a_*^2 \cos^2 i, \quad (26)$$

which follows by adding the squares of α and β . For an exactly axial observer ($i = 0$) the critical curve is a circle of radius ρ , and the requirement that β remain real in the limit forces $\xi \rightarrow 0$ (equivalently $L_z = 0$): otherwise the $-\xi^2 \cot^2 i$ term in (25) would dominate and drive β^2 negative.

With $\xi \rightarrow 0$ enforced by the polar limit, the axial shadow radius is fixed by the unique spherical photon orbit on which $\xi(r)$ vanishes. Denoting its Boyer-Lindquist radius by r_0 , we obtain

$$\rho_{\text{pole}}(a_*) = \sqrt{\eta(r_0) + a_*^2}, \quad \xi(r_0) = 0. \quad (27)$$

Using (22), the condition $\xi(r_0) = 0$ reduces to a single cubic equation,

$$r_0^3 - 3r_0^2 + a_*^2 r_0 + a_*^2 = 0, \quad (28)$$

and the physical root is selected as the one that lies in the admissible spherical-orbit interval $r_0 \in [r_-, r_+]$ and connects continuously to the Schwarzschild value $r_0(0) = 3$. The axial shadow is then a circle of area

$A_{\text{pole}} = \pi \rho_{\text{pole}}^2$ and diameter $D_{\text{eq,pole}} = 2\rho_{\text{pole}}$, so that

$$A_{\text{pole}} = \pi \rho_{\text{pole}}^2, \quad D_{\text{eq,pole}} = 2\rho_{\text{pole}}, \quad (29)$$

$$y_{\text{pole}}(a_*) = \frac{D_{\text{eq,pole}}}{6\sqrt{3}M} = \frac{\rho_{\text{pole}}}{3\sqrt{3}M}. \quad (30)$$

In practice we avoid the coordinate degeneracy of the screen map by taking our dense validation set to start at a small but nonzero inclination $i \geq i_{\min}$. If one nevertheless wishes to include $i = 0$ in a reference grid, it should be evaluated through (27)-(30) rather than through the direct (α, β) map.

The celestial-coordinate relations (24)-(25) are standard; for definiteness we follow the conventions of Ref. [17]. For each allowed spherical radius r they produce two points on the screen, corresponding to the upper and lower branches $\beta_{\pm}(r)$, which together form the closed critical curve.

To parametrize the critical curve we sample spherical radii r between the prograde and retrograde equatorial photon-orbit radii, $r_- \leq r \leq r_+$. These endpoints have the closed forms

$$r_- = 2 \left[1 + \cos\left(\frac{2}{3} \arccos(-a_*)\right) \right], \quad (31)$$

$$r_+ = 2 \left[1 + \cos\left(\frac{2}{3} \arccos(+a_*)\right) \right]. \quad (32)$$

For $a_* = 0$ both reduce to $r_{\pm} = 3$, as expected.

Choose an integer $N_r \geq 2$ and sample radii $\{r_j\}_{j=1}^{N_r}$ on $[r_-, r_+]$ (in our implementation we take them uniformly in r). For each r_j compute $(\xi_j, \eta_j) = (\xi(r_j), \eta(r_j))$ from (22)-(23), and then map to the observer screen using (24)-(25) to obtain $(\alpha_j, \beta_{j,+})$ and $(\alpha_j, \beta_{j,-})$.

The only numerical subtlety enters through the radicand in (25). Writing

$$B^2(r) \equiv \eta(r) + a_*^2 \cos^2 i - \xi(r)^2 \cot^2 i,$$

we occasionally encounter small negative values of B^2 caused by floating-point roundoff near the boundary of the admissible set. We handle this in a scale-aware way: if $B^2 < 0$ but

$$|B^2| \leq \tau(|T_1| + |T_2| + 1), \quad T_1 = \eta + a_*^2 \cos^2 i, \quad T_2 = \xi^2 \cot^2 i,$$

we set $B^2 \leftarrow 0$; otherwise the point is rejected as non-physical. In all computations reported in the main text we use $\tau = 10^{-10}$.

To obtain an ordered closed polygon without any angle-sorting heuristics, we traverse the critical curve in a fixed way: we follow the upper branch in increasing r and return along the lower branch in decreasing r , i.e.

$$(\alpha_1, \beta_{1,+}), \dots, (\alpha_{N_r}, \beta_{N_r,+}), (\alpha_{N_r}, \beta_{N_r,-}), \dots, (\alpha_1, \beta_{1,-}).$$

This concatenation fixes the vertex ordering deterministically and is robust across the full (a_*, i) domain with $i > 0$.

Given the ordered vertex list $\{(\alpha_k, \beta_k)\}_{k=1}^N$ with $N = 2N_r$, we compute the enclosed area by the shoelace formula,

$$A = \frac{1}{2} \left| \sum_{k=1}^N (\alpha_k \beta_{k+1} - \alpha_{k+1} \beta_k) \right|, \quad (33)$$

$$(\alpha_{N+1}, \beta_{N+1}) \equiv (\alpha_1, \beta_1), \quad (34)$$

and then define the equivalent diameter by

$$D_{\text{eq}} = 2\sqrt{\frac{A}{\pi}}. \quad (35)$$

As a simple sanity check, in the Schwarzschild case $a_* = 0$ the critical curve is a circle of radius $3\sqrt{3}$ on the screen, so $A = 27\pi$ and $D_{\text{eq}} = 6\sqrt{3}$. For $i \rightarrow 0$ at fixed $a_* \neq 0$ the curve is again circular but with a spin-dependent radius. This dependence is encoded in the polar function $y_{\text{pole}}(a_*)$ used throughout the main text.